stellarator news

Published by Fusion Energy Division, Oak Ridge National Laboratory
Building 9201-2; P.O. Box 2009; Oak Ridge, TN 37831-8071, USA
Editor: James A. Rome Issue #31 January 1994
E-Mail: jar@ornl.gov Phone: (615) 574-1306

## Around the Labs

# Performance of Heliotron-E ECH plasma after boronization

Boronization has been successfully applied in Heliotron-E since July. A thick layer of boron (about 100–200 nm thick) was deposited by using a 2.45-GHz electron cyclotron heating (ECH) discharge with helium and $B_{10}H_{14}$. The ECH discharge deposits the boron uniformly in the torus.

After the boronization, ECH experiments were carried out by using three 53.2-GHz gyrotrons. The maximum pulse width was 100 ms and the total launched power was up to 400 kW. The parameter range of the ECH plasma was extended by increasing the heating power. In the previous experiments before the boronization, the quasi-steady plasma near the cut-off density ($\langle n_e \rangle = 3.5 \times 10^{13}$ cm$^{-3}$) could be obtained only when the launched power was more than 640 kW [1]. The high-temperature regime was restricted by a critical value of $P_{ECH}/\langle n_e \rangle$. After the boronization, a plasma with a high density, up to cut-off density, was attainable using only 400 kW of ECH power. The radiation was suppressed, and the impurities like O-V were reduced at the high density. Figure 1 shows the density dependence of $T_e(0)$ and $T_i$, which were measured with a Thomson scattering system and a neutral particle analyzer, respectively. The maximum of $\langle n_e \rangle T_e(0)$ was obtained at $\langle n_e \rangle \sim 2.8 \times 10^{13}$ cm$^{-3}$. Diamagnetic measurement also showed that the stored energy had a maximum value $W_p = 4$ kJ at $\langle n_e \rangle \sim 3.0 \times 10^{13}$ cm$^{-3}$. The $n_e$ profile was flat, and the peaking factor $n_e(0)/\langle n_e \rangle$ was about 1.1 over the operational density region.

After the boronization, global magnetohydrodynamic (MHD) instabilities were observed in limiter-inserted ECH plasmas with low beta [$\beta(0) \lesssim 0.1\%$]. Similar instabilities have been observed in low beta [$\bar{\beta} \lesssim 1\%$] neutral

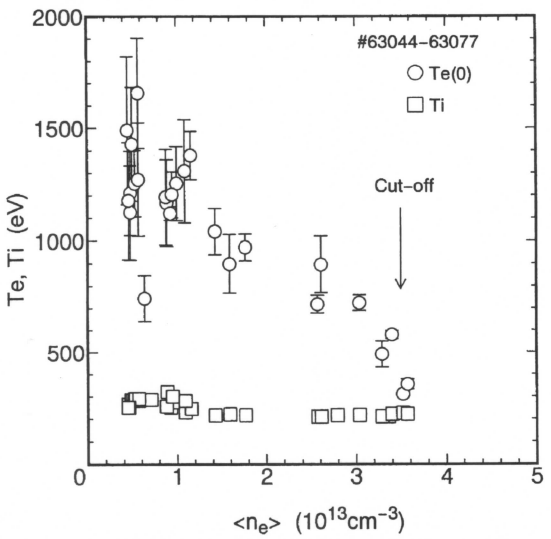


**Fig. 1.** $n_e$ dependence of temperature, $T_e(0)$ and $T_i$ after boronization. ECH power is 350–400 kW.

beam injection (NBI)-plasmas when the limiter is inserted [2]. The rail-type graphite limiter mixed with $B_4C$ is inserted from the bottom of the torus. When the limiter is located at $z = -16$ cm ($r_{Lim}/a = 0.57$, $\iota_{Lim} = 0.86$), the sawtooth oscillation appears as shown in Fig.2. Here $z$ is the vertical position of the limiter, $r_{Lim}$ is averaged plasma minor radius at the limiter head, $a$ is the minor radius of the last closed flux surface without the limiter, and $\iota_{Lim}$ is rotational transform at the limiter head. The plasma predominantly interacts with the limiter so that the MHD instability can be hardly detected in the wall $H_\alpha$ emission and the probe signal at the divertor region like the ion saturation current. Although $T_e(0)$ gradually decreases as the limiter is inserted, it is still high, $T_e(0) \sim 800$ eV, when the limiter is located at $r_{Lim}/a = 0.57$.

FFT analysis for magnetic fluctuations shows that the dominant mode is $m = 3$, the mode frequency is 10 kHz, and the poloidal rotation is in the ion diamagnetic direction. When the limiter is located at $z = -14$ cm ($r_{Lim}/a = 0.50$, $\iota_{Lim} = 0.77$), the frequency of the sawtooth becomes higher. The limiter insertion can change the pressure profile in the boundary region of the plasma. The steep pressure gradient drives an interchange instability

at rational surfaces. In this case, the interchange mode is destabilized at $\iota = 2/3$. Further limiter insertion ($z = -1$ cm, that is, $r_{Lim}/a = 0.43$, $\iota_{Lim} = 0.70$) did not trigger the sawtooth oscillation. Although the MHD coherent modes were not identified during the heating phase at $z = -18$ cm ($r_{Lim}/a = 0.64$, $\iota_{Lim} = 0.97$), $m = 4$ magnetic fluctuations were enhanced during the decay phase after the ECH had been turned off. Detailed analysis of these MHD instabilities is under way.

K. Nagasaki, H. Zushi, and the Heliotron-E Group
Plasma Physics Laboratory, Kyoto University
Gokasho, Uji, Kyoto, 611, Japan

Phone: +81-774-31-8130
FAX: +81-774-33-0865

REFERENCES

[1]. O. Motojima et al., in *Plasma Physics and Controlled Nuclear Fusion Research* (IAEA, Nice, 1988) **1** (1989) 551.

[2]. S. Sudo et al., J. Plasma and Fusion Research **69**, 1208 (1993).

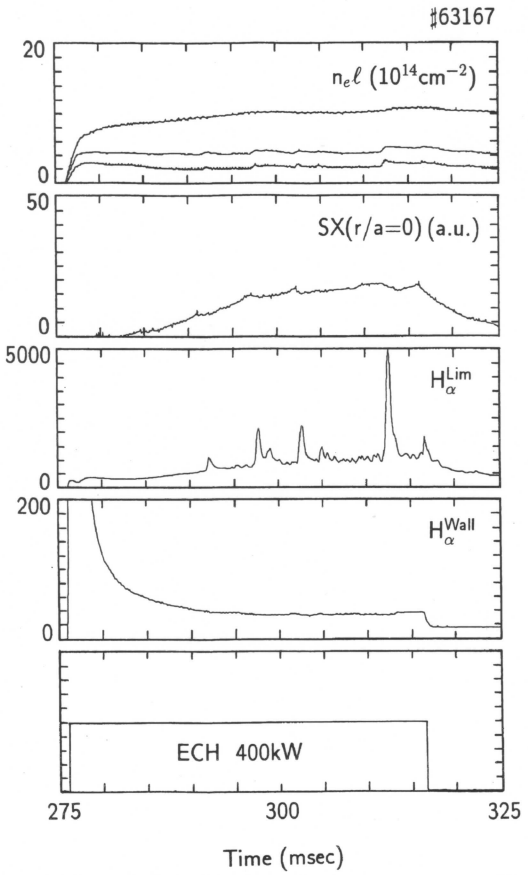


**Fig. 2.** Global MHD instability in a limiter-inserted ECH plasma. The limiter position is $z = -10$ cm ($r_{Lim}/a = 0.57$). The sawtooth oscillation can be seen in peripheral FIR chords, soft X-ray, and $H_\alpha$ emission at the limiter.

## Shafranov shift in the W7-AS stellarator at low iota and varied "mirror ratio"

The Shafranov shift in W7-AS is known to be reduced by a factor of about 2 in value in comparison to conventional stellarators, such as the former Garching stellarator Wendelstein 7-A. Due to a partial optimization of the vacuum magnetic field, the Pfirsch-Schlueter currents, which are causing the shift are also reduced in W7-AS by the same factor of 2. The reduced Shafranov shift has been demonstrated by soft X-ray profile analysis [1] in comparison with equilibrium calculations using the KW code [2], as summarized in *Stellarator News* #16 (1991). Considerably smaller displacements are seen at increased iota values, as expected.

The present contribution is concerned with free-boundary calculations of W7-AS equilibria at low iota and varied "toroidal mirror ratio," using the NEMEC code, which consists of the VMEC code [3] in combination with the NESTOR code [4]. Net-current-free plasmas are considered at different pressure profiles, mainly linear in the normalized toroidal flux, i.e., parabolic in true space.

Three types of low-iota configurations of W7-AS are compared. They differ mainly in the principal components of the Fourier coefficients $B(m,n)$ of the magnetic field strength, where $m$ is the poloidal harmonic number, and $n$ is the toroidal harmonic number divided by the field period. The Standard case "S" has a small field ripple on the axis with approximately $B(0,1)/B(0,0) = -B(0,2)/B(0,0) = 1\%$. The other two configurations have an enhanced "toroidal mirror ratio" but differ in the phase of the field modulation. In the "R"-configuration, characterized by $B(0,1)/B(0,0) = -10\%$ and $B(0,2)/B(0,0) = 2\%$, the maximum axis field strength is in the "elliptical" plane, $\phi = 36°$, the plane of ECRH power input for plasma start-up; the alternative "A"-configuration with $B(0,1)/B(0,0) = 10\%$ and $B(0,2)/B(0,0) = -4\%$ has a minimum there. Initial plasma experiments in such configurations were discussed in Ref. 5; the effect of a varied mirror ratio on the electron cyclotron current drive was commented on in *Stellarator News* #29 (1993).

The vacuum fields used for the finite-beta calculations include a vertical field to achieve some inward shift of the magnetic axis. Various values of the average major radius are chosen with approximately the above-given mirror ratios and having the same value of the edge rotational transform, $\iota_a \sim 0.34$. The limiter positions have been set up to give the same average minor radius $a =$

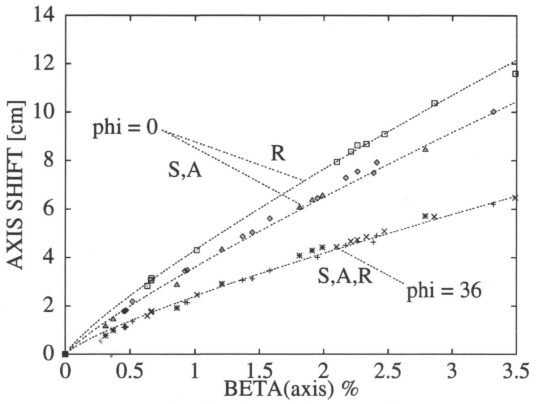


**Fig. 3.** Axis shift calculated for the three low-iota configurations of W7-AS with the free boundary code NEMEC. The inward-shifted vacuum fields have values of 1.27 T on axis at the elliptical plane. Thus, the average fields differ for the three cases. Top curve "R," triangular plane; middle curve "A" and "S," triangular plane; bottom curve "A," "S," and "R," elliptical plane. The largest shift is seen for the triangular plane in the "R" configuration.

zontal extension of the flux surfaces is larger, exhibit larger shifts at the same beta value. About 8 cm are found for the configuration types "S" and "A," and 9 cm for the "R" configuration (top curve). A broad pressure profile with nearly the same value of beta(axis) yields about the same values of the axis shift as a peaked one, but introduces a larger shift of the free plasma boundary. This feature was seen in all three configurations.

The toroidal modulations of the magnetic field on axis are nearly maintained under finite beta in the three configuration types. It is small for the standard configuration, which yields an average of 1.24 T, with a small dip near $\phi = 36°$. Typical values for the "R" configuration are an increase from 1 T at $\phi = 0°$ to a maximum of 1.2 T at $\phi = 36°$ for a parabolic pressure profile with beta(axis) = 2.2%, and a decrease from 1.5 to 1.2 T in the "A" configuration at beta(axis) = 1.8%.

These calculations serve as a basis for the evaluation and interpretation of experimental results in the three configuration types of W7-AS. Of importance in this respect is the transformation of flux coordinates of the finite-beta code to the three-dimensional spatial coordinates of the various diagnostics. After initial start-up with ECRH, finite-beta plasmas were produced with the use of four NBI sources at a total power of about 1 MW. Preliminary results of volume-averaged beta values range between 1 and about 1.2% for these experiments.

J. Geiger and F. Rau
IPP Garching, Germany
E-mail FFR@IBMA.IPP-GARCHING.MPG.DE

Phone: 049-89-3299-1770
FAX: 049-89-3299-2579

REFERENCES

[1] A. Weller et al., Proc. 17th EPS Conf. Amsterdam 1990, Europhysics Conf. Abstr. **14b**, Pt. II, 479.

[2] J. Kisslinger and H. Wobig, Proc. 12th EPS Conf. Budapest 1985, Europhysics Conf. Abstr. **9f**, Pt. I, 453.

[3] S. P. Hirshman and J.C. Whitson, Phys. Fluids **26**, 3553 (1983).

[4] P. Merkel, J. Comput. Phys., **66**, 83 (1986).

[5] F. Rau et al., Proc. 20th EPS Conf. Lisbon 1993, Europhysics Conf. Abstr. **17c**, Pt. I, 341.

## LHD Helical Coil Superconductor has been developed

The National Institute for Fusion Science (Toki, Gifu, Japan) has been constructing a fully superconducting Large Helical Device (LHD) since 1990. The most difficult technological aspect is to guarantee the stability of the superconducting helical coils because of their large stored energy and the complicated structure from the viewpoint of electromagnetic force. Since 1989, we have been developing a fully stabilized superconductor for the helical coils, using the world's largest superconducting coil test facility. The facility at Toki has a 75-kA current supply, a 9 T split coil, and a 1000-ton mechanical testing machine. In 1993, we finally succeeded in the development of a superconductor that will meet the required specifications for the LHD helical coils.

The procedure of the superconductor test experiment is as follows. Figure 1 shows a schematic drawing of the typical sample for the conductor tests. Two conductors, each 2 m long, were soldered together at the bottom. The sample was vertically inserted into the split coil, which has a 90% flat top region of about 250 mm. Voltage taps were attached on the conductor surface to measure the normal resistance in the longitudinal direction and to measure the perpendicular voltages related to the Hall effect. The surface temperatures were also measured. The exposure rate of conductors was 50% using the GFRP spacers in the standard test condition.

Several types of superconductors have been proposed and tested between 1989 and 1992. They were bath-cooled composite-type superconductors with NbTi superconducting strands and copper and pure aluminum

15.4 cm for all cases. The vacuum field strength on axis is determined by the resonance condition of ECRH launch, 1.25 T at $\phi = 36°$ on axis. Thus, the three types of vacuum fields have different average field values on the axis, the lowest ones being for the case "R" with $B(36°) = MAX$.

The finite-beta calculations are extended up to peak beta values of 3.5%, i.e., beyond those obtained experimentally in W7-AS at low iota so far. As an example, Fig. 1 compares vacuum flux surfaces (dashed) and the finite-beta topology of the "R" configuration at a value of beta(axis) = 2.2% and a parabolic pressure profile in space. The resulting shift of the magnetic axis is visible in the figure and exceeds that of the free boundary (outmost magnetic surface shown). The triangularity at $\phi = 0°$ (upper part of the figure) is enhanced; the vertical extension at the elliptical plane, $\phi = 36°$, is nearly maintained. The steepest gradients in the figure occur at the outboard side of the shifted profile.

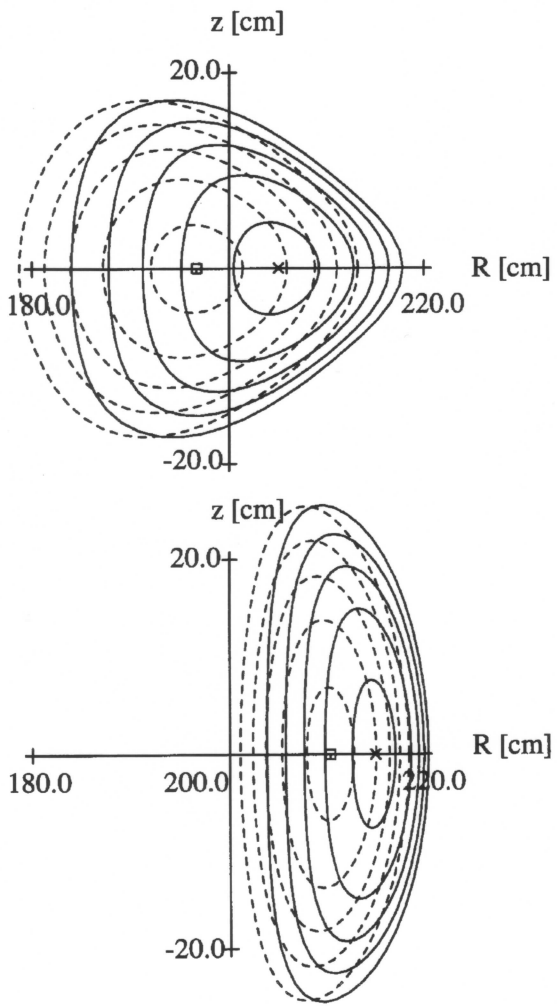


**Fig. 1.** Flux surfaces of the "R" configuration and shift of the magnetic axis at beta(axis) = 2.2% with a parabolic profile in space. Free-boundary code NEMEC is operated with an average minor radius $a$ = 15.4 cm of the initially inward-shifted vacuum field. Dashed curves: vacuum field; solid curves: finite-beta. Upper part: $\phi = 0°$, lower part $\phi = 36°$. Further details are commented on in the text.

Another effect of the finite plasma pressure is a change of iota and shear. For beta(axis) = 2.2% with a parabolic pressure profile, the axis value of iota for the "R" configuration rises from 0.33 to 0.39 whereas the edge value, evaluated at an average minor radius of 15.4 cm, is reduced from 0.34 to 0.29, when comparing the initial vacuum field data and the results of the NEMEC code (see Fig. 2.) The positive shear in the vacuum field of this configuration type is reversed for the above finite-beta data.

The two other configurations also have negative shear at finite beta. Their vacuum fields have small shear in the standard case and negative shear in the "A" configuration. The increase of the iota value on axis is smallest in the "R" configuration at finite beta for a given beta profile.

Fig. 3 is a summary of the calculations performed for the three cases. As is known for other stellarators, the Shafranov shift of the axis is smallest for the toroidal angle where the magnetic surfaces are vertically elongated, i.e., at $\phi = 36°$ in W7-AS. It amounts to 5 cm at beta(axis) = 2.5% (lowest curve of the figure). No difference appears to be present for the three configuration types. This is due to the fact that the horizontal extensions of the flux surfaces differ only very slightly for the three configurations. In addition, the magnetic field value on axis was fixed to the same value for the vacuum fields. The triangular planes, $\phi = 0°$, where the hori-

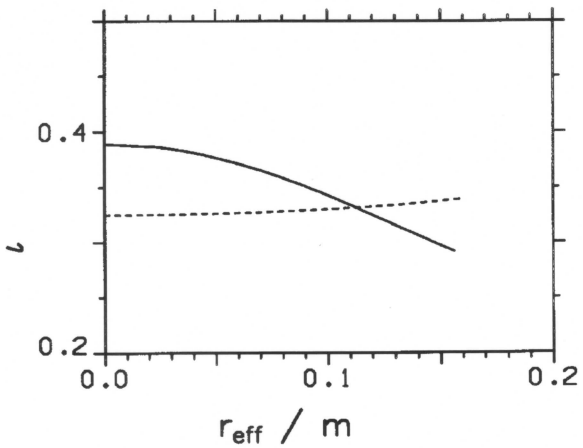


**Fig. 2:** Radial profile of the rotational transform for the calculation of the previous figure. Dashed curve: vacuum field; solid curve: finite-beta.

stabilizers. Critical current and stability characteristics were mainly investigated. The measured critical currents were in good agreement with the values predicted from the measured critical current of each strand. On the other hand, the recovery currents were much less than the expected values in all conductors. By analyzing data of several conductors with different internal structures, the resistivity of the aluminum stabilizers was found to be quite a bit higher than the expected values under a high magnetic field. It was concluded that the cause was anomalous magnetoresistivity due to the Hall effect; this appears in metal-metal composites with different resistivities and different Hall coefficients.

The final superconductor was developed in 1993. It has a nominal current of 13 kA at 7 T with a cross section of 12.5 by 18 mm. The size of the conductor was reduced from the original design of 19 mm square with a nominal current of 21.2 kA to increase the heat transfer from the conductor surface to the liquid helium. The cross-sectional view of the superconductor is shown in Fig. 2. The aluminum stabilizer is co-extruded with Cu-2%Ni cladding to reduce the Hall effect, which was one of the main improvements that resulted from the conductor R&D. The critical current was 21 kA at the bias field of 7 T (the self-field effect must be taken into account), and the recovery current was 13 kA at 7 T, as shown in Fig. 3. The conductor surface is oxidized to improve the heat transfer coefficient. The copper sheath was electron beam welded to ensure the mechanical toughness.

As preparation for the coil winding, we are testing the effect of strain on a conductor after coil winding, evaluating coil connection techniques, and measuring the heat transfer with actual spacers. The conductor is ready for coil fabrication, which will be performed at the Toki site starting in the summer of 1994.

Junya Yamamoto and Nagato Yanagi
National Institute for Fusion Science
Nagoya 464-01, Japan

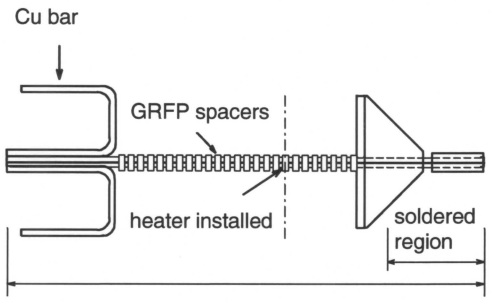


**Fig. 1.** Short sample design of helical superconductor test.

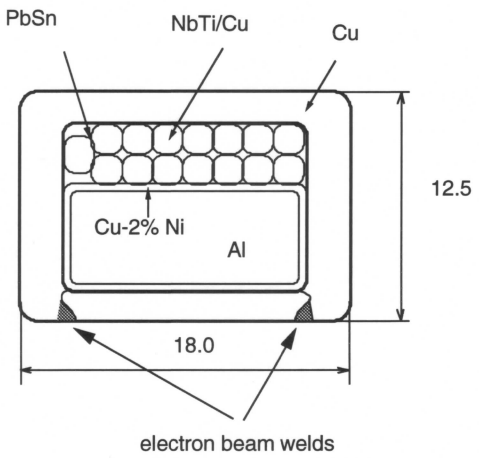


**Fig. 2.** Cross-section of the superconductor.

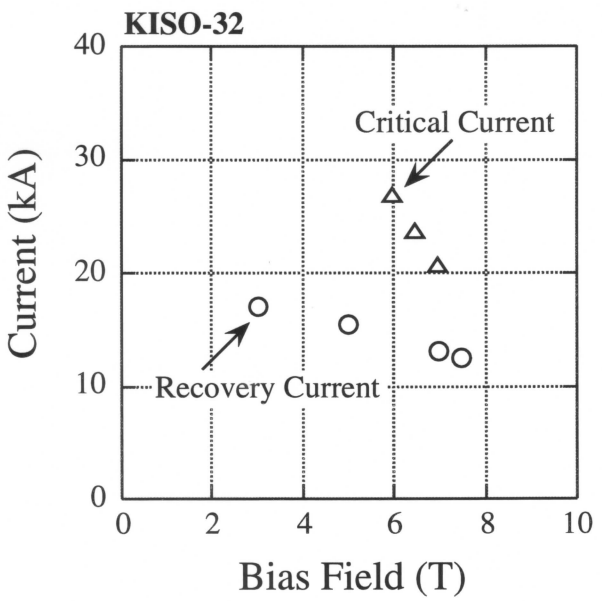


**Fig. 3.** Critical and recovery current of the conductor under magnetic field.